Published in final edited form as:
J Control Release. 2007 August 28; 121(3): 190–199. doi:10.1016/j.jconrel.2007.06.006.

Nanolayer Biomaterial Coatings of Silk Fibroin for Controlled Release

Xianyan Wang[1], **Xiao Hu**[4], **Andrea Daley**[1], **Olena Rabotyagova**[1,2], **Peggy Cebe**[4], and **David L. Kaplan**[1,3,*]

1 *Department of Biomedical Engineering, Tufts University, Medford, Massachusetts 02155, USA*

2 *Department of Chemistry, Tufts University, Medford, Massachusetts 02155, USA*

3 *Department of Chemical and Biological Engineering, Tufts University, Medford, Massachusetts 02155, USA*

4 *Department of Physics and Astronomy, Tufts University, Medford, Massachusetts 02155, USA*

Abstract

An all-aqueous, stepwise deposition process with silk fibroin protein for the assembly of nanoscale layered controlled release coatings was exploited. Model compounds, Rhodamine B, Even Blue and Azoalbumin, representing small molecule drugs and therapeutically relevant proteins were incorporated in the nanocoating process and their loading and release behavior was quantified. In addition, the structure and morphology of the coatings were characterized. Release studies *in vitro* showed that control of *β*-sheet crystal content and the multilayer structure of the silk coatings correlated with the release properties of the incorporated compounds. In particular, higher crystallinity and a thicker silk capping layer suppressed the initial burst of release and prolonged the duration of release. These novel coatings and deposition approach provide a unique option to regulate structure and morphology, and thus release kinetics. The results also suggest these systems as a promising framework for surface engineering of biomaterials and medical devices to regulate the release of drugs, when considered with the all-aqueous process involved, the conformal nature of the coatings, the robust material properties of silk fibroin, and the degradability and biocompatibility of this family of protein.

Keywords

controlled release; silk fibroin; nanolayers; biomaterials

1. Introduction

There is a critical need in medicine to develop simple and versatile methods to assemble robust, biocompatible and functional biomaterial coatings that direct cellular outcomes. Toward this goal, layer-by-layer (LbL) thin film assemblies have been investigated for drug release surface engineering in recent years due to the ability to control the composition of these films with

*David L. Kaplan, Department of Biomedical Engineering, 4 Colby St., Medford, Massachusetts 02155, U.S.A., Tel: 617-627-3251, Fax: 617-627-3231, E-mail: david.kaplan@tufts.edu.

nanometer precision, and to incorporate a range of functional biomolecules, including small molecules, peptides, proteins, heparin, and enzymes without substantial loss in activity.[1,2,3,4] In addition, this LbL approach is relatively simple in terms of a fabrication process and can be utilized to coat almost any surface or device because of the all aqueous processing and conformal fits.[5] Conventional LbL is based on the alternating deposition of oppositely charged polyelectrolytes, forming interpenetrating layers of polymeric complexes.[6,7]

The release of compounds entrapped in the process has been primarily induced by disrupting the multilayer structure by changing pH or ionic strength with high salt concentrations. Chung *et al.* demonstrated the triggered release of methylene blue from a weak polyelectrolyte multilayer film, poly(acrylic acid)/poly(allylamine hydrochloride), initiated by changing the pH in the range of 2.0 to 6.5.[8] Sukhishvili *et al.* also demonstrated that Rhodamine 6G could be released from a polyacid/polybase multilayer system formed by hydrogen bonding, by changing the pH and ionic strength of the environment.[9] Neither of these approaches is particularly suitable to physiological conditions for controlled release, and some of these conditions can reduce the function of sensitive biological molecules that may be desired for delivery. Recently, a hydrolytically degradable poly(*β*-amino ester) thin coating system for controlled release of heparin under physiological conditions was described.[10] In another study, a conducting polymer, poly(anilineboronic acid), was used to immobilize RNA.[11] The release of RNA from these multilayer thin films was controlled electrochemically under neutral pH condition. These methods offer alternatives to previously reported methods in that they are more compatible with *in vivo* delivery and control. However, limitations with these recent alternative methods remain in terms of synthesis, biocompatibility and controlled rates of degradation of the polymers.

In our recent report, we demonstrated that nanoscale thin coatings of silk fibroin could be formed by stepwise deposition using an all aqueous process.[12] The silk fibroin protein adsorbed onto various substrates spontaneously and the thickness and structure of the silk coatings could be controlled by changing the composition of the dipping solution and coating dehydration method. In addition, unlike conventional LbL techniques which require appropriate charges or functional groups for the buildup of coating layers, the structural control of the silk protein locks in the features of the coatings due to physical crosslinks (*β*-sheet crystals), resulting in robust and stable material coatings that do not require specific chemical or photoinitiated crosslinking reactions. In recent work we observed outstanding mechanical properties for ultrathin silk films, with thickness below 100 nm, prepared by spin-assisted LbL deposition (manuscript in preparation). The mechanical parameters were close to or exceeded those of reinforced polymeric nanocomposites and some high-performance polymers both in compressive and tensile modes. These films were characterized by a high elastic modulus of 6.5 GPa and ultimate strength reaching 100 MPa. These properties were due to the formation of reinforced microstructures with crystalline *β*-sheets serving as the reinforcing fillers and physical crosslinks.

Silks represent a new family of advanced biomaterials due to their unique attributes of high mechanical strength and excellent biocompatibility. Comprehensive studies, both *in vitro* and *in vivo*, have demonstrated that silk fibroins are more biocompatible than other commonly used polymeric degradable biomaterials, such as PLA, PGA and collagen.[13,14,15] Another important attribute of silks is their processability into different material formats, such as films, gels, nanofibrous membranes and 3-dimensional porous scaffolds, with control of crystalline state (*β*-sheet content) and morphology to modulate the rate and extent of degradation.[16,17,18,19] The excellent biocompatibility and the ability to control the structural and morphological features of silk proteins in an all-aqueous process render this family of proteins as important candidates for controlled release. The control of the silk fibroin structure and morphology could be utilized to regulate the release kinetics of the incorporated compounds. The efficacy of silk

fibroin aqueous solution cast films as delivery vehicles for bioactive compounds has been studied using horseradish peroxidase (HRP) and lysozyme (Lys) as model protein drugs.[20] The controllable levels of crystallinity of silk fibroin render itself as an interesting polymer for drug delivery. Silk fibroin aqueous solution was also used as a coating material for theophylline tablets to achieve sustained drug release by varying the number of coatings and the degree of cross-linking of silk fibroin with polyethylene glycol.[21] Other applications of silk fibroin as polymer matrix for controlled release of model drugs, such as theophylline, diclofenac sodium, amoxicillin trihydrate, and salicylic acid have also been reported.[22,23]

In the present study, thin silk fibroin coatings were prepared through the stepwise deposition process and utilized as carriers to incorporate model drugs. Organic dyes, Rhodamine B (479 Da) and Even Blue (965 Da), were used as model compounds for small molecule drugs. Azoalbumin (~69 kDa), a bovine serum albumin derivative containing an azo group, was used as a model to represent therapeutically relevant proteins like growth hormones, erythropoietin and interferons. These model compounds can be easily traced visually as well as assayed spectrophotometrically due to their characteristic absorbance spectra. The primary focus of the study was to determine the feasibility of immobilization of a variety of molecules and to control their release kinetics via control of the structure of the silk coatings deposited by LbL assembly. UV-Vis spectroscopy and quartz crystal microbalance (QCM) were employed to monitor the stepwise deposition process and quantify the release of model compounds. Wide angle X-ray diffraction (WAXD) and atomic force microscopy (AFM) were used to characterize the structure and morphology of the fibroin coatings, respectively. Various approaches to modify drug release profiles are described and the applicability of silk multilayer thin films in drug delivery is discussed.

2. Experimental Section

2.1. Materials

Cocoons of *B. mori* silkworm silk were kindly supplied by M. Tsukada, Institute of Sericulture, Tsukuba, Japan. All other chemicals were of analytical or pharmaceutical grade and purchased from Sigma and Aldrich (St. Louis, MO) and used without further purification. The structures of the small molecule model compounds, Rhodamine B and Even Blue, are shown in Figure 1. Azoalbumin is a bovine serum albumin covalently linked to sulfanilic acid, with a single polypeptide chain consisting of about 583 amino acid residues.

Silk fibroin aqueous stock solutions were prepared as previous described.[24] Briefly, cocoons of *B. mori* were boiled for 20 min in an aqueous solution of 0.02 M Na_2CO_3, and then rinsed thoroughly with distilled water to extract the glue-like sericin proteins. The extracted silk fibroin was then dissolved in 9.3 M LiBr solution at 60°C for 4 h, yielding a 20% (w/v) solution. This solution was dialyzed against distilled water using a Slide-a-Lyzer dialysis cassette (MWCO 3,500, Pierce) at room temperature for 48 h to remove the salt. The dialysate was centrifuged 2 times, each at −20°C for 20 min to remove impurities and the aggregates that formed during dialysis. The final concentration of silk fibroin aqueous solution was approximately 8% (wt/v). This concentration was determined by weighing the residual solid of a known volume of solution after drying at 60°C for 24 h.

Silk solutions used for dipping were prepared by diluting the stock silk solution with deionized (DI) water to a concentration of 2 mg/ml. Rhodamine B and Even Blue dipping solutions were prepared with DI water at concentrations of 0.5 to 2.0 mg/ml depending on the sequential experiments. Azoalbumin dipping solution was prepared with phosphate-buffered saline (PBS) buffer ((pH 7.4, 137 mM NaCl, 2.7 mM KCl, 10 mM Na_2HPO_4) and at concentration of 0.5 to 2.0 mg/ml. Different substrates were used for film deposition depending on the method of characterization. Quartz microscope slides for UV-Vis spectroscopy measurements were from

Quartz Scientific, Inc. (Fairport Harbor, OH), and glass microscope slides for release study were from VWR Scientific (Bridgeport, NJ). Quartz crystals with evaporated gold electrodes for the research quartz crystal microbalance (RQCM) measurements were from Maxtek, Inc. (Cypress, CA). Freshly cleaved mica for atomic force microscope (AFM) measurements was from Ted Pella, Inc.(Redding, CA). Silicon wafer for X-ray diffraction study was from Montco Silicon Technologies, Inc. (Spring City, PA). It should be noted that variations in deposition may occur when different substrates are used. The substrates were cleaned by sonication for 2 h in 1% Chemsol solution from Mallinckrodt Chemicals (Phillipsburg, NJ) and thoroughly rinsed with deionized water and dried under a stream of nitrogen gas. Deionized water (18 MΩcm) was used in all washing steps and to prepare silk fibroin and organic dye compound solutions.

2.2. Preparation of model compound- incorporated multilayer films

The buildup of the multilayers was accomplished by consecutive adsorption of silk fibroin and the model compounds using an optimal dipping protocol similar to that previously reported.[12] Briefly, the cleaned substrate was immersed in the silk dipping solution (2 mg/ml) for 2 or 5 min depending on the subsequent studies at room temperature followed by rinsing with deionized water or methanol/water (90:10 v/v) for 1 min. After the deposition and rinsing steps, the substrate was dried with a gentle flow of dry nitrogen gas for 2 min. At the second step, the silk fibroin-coated substrate was immersed in the model molecule aqueous solution (0.5 or 2.0 mg/ml) for 2 minutes. When preparing samples for the release study, a 5 min dipping time and a concentration of 2.0 mg/ml for model compounds was used. This process was repeated according to the designated multilayer structure in which the outmost layer was always silk layer. In this work, two different loading modalities were used in the release study for each compound, each with two different rinsing methods as shown in Table 1. The rationale of using more barrier layers for small molecules than that for protein was based on the presumption that small molecules have higher diffusion rates. With this approach, a comparable duration of complete release for small molecules and proteins could be achieved.

2.3. Multilayer coating characterization

The buildup of the multilayers on quartz slides was monitored using the characteristic absorbance of silk fibroin and the model compounds at each deposition by PerkinElmer Lambda spectrophotometer. Real time deposition of model compounds on silk-coated electrode was recorded by RQCM. AFM images were acquired by a Digital Instrument Dimension 3000 in tapping mode for the characterization of the surface morphology of the coatings before and after incubation in PBS for 24h and for the thickness of the films. The structures of the coatings were analyzed with a Bruker D8 Discover X-ray diffractometer with GADDS multiwire area detector employing Cu Kα radiation ($\lambda_{k\alpha}$ = 0.154 nm, 40 kV and 20 mA) and 0.5 mm collimator. Sodelite standard reference powder was used to calibrate the q-vector ($q = 4\pi\sin\theta/\lambda$ for θ the half-scattering angle) for the angular range from 2θ = 5°–60°. The scattering invariant, Q, was obtained from the total integrated area under the Lorentz-corrected intensity, $I(q)q^2$ curve: $Q = \int I_{corr}(q)\, q^2\, dq$, where I_{corr} is the scattered intensity after all corrections have been applied.[25,26] The amorphous baseline area, Q_a, and the crystalline area, Q_c, were determined from: $Q_a = \int I_a q^2 dq$ and $Q_c = Q - Q_{a,}$, where I_a is the intensity of the amorphous peak. The WAXS crystallinity index X_c is defined as $X_c = Q_c/Q$.[27]

2.4. In vitro release study

The compound release from the multilayer coatings on glass microscope slides (25 × 75 mm on both sides) was investigated by incubating the slides in 5 ml PBS buffer solutions at room temperature with gentle shaking (60 rpm). At preset time intervals, 2 ml supernatant was sampled and 2 ml fresh PBS solution was then added to replenish the sample that was removed

in order to maintain a constant volume. The supernatant was analyzed for the amount of released model compound using UV-Vis spectroscopy for optical densities at a specific wavelength for each compound (562 nm for Rhodamine B, 609 nm for Even Blue, and 358 nm for Azoalbumin) and compared to a standard curve generated for each compound. The amount of released compound in each sample was summed with the amounts at each previous time point and divided by the total amount to obtain cumulative release value. Experiments were run in triplicates (n=3). Data in the graphs represent the average ± standard deviation.

3. Results and Discussion

3.1. Assembly of silk-model compound multilayer films

UV-vis spectroscopy is conventionally used to evaluate the deposition process of optical active multilayers[28,29] and was used in the present work to monitor the incorporation of the model compounds. Figure 2a and 2b show representative UV-Vis spectra of assembled $(silk/RH)_n$ and $(silk/AA)_n$ on quartz slides measured at each cycle (a cycle corresponding to a silk/compound bilayer). The inset shows that the absorbance of the peaks at 562 nm and 359 nm (characteristic absorption peaks of the Rhodamine B and Azoalbumin) increases almost monotonically with the number of bilayers, substantiating the incorporation of the model compounds into the silk film. The linear relationships indicate that the films were uniformly assembled layer-by-layer on the quartz substrate. Thus it is possible to precisely control the amount of material deposited simply by controlling the number of layers that are dip coated.

Similarly, adsorption for the model compounds also proceeded linearly while rinsing the films with methanol/water (90/10 v/v) at each step but with a significantly higher increment (up to 38%) for each step of deposition when prepared from a silk solution and a model compound solution of the same concentrations. The comparison of absorbance at 562 nm for Rhodamine-incorporated films at each dipping cycle using two different rinsing methods is shown in Figure 3. At each dipping cycle, the absorbance of the films prepared by rinsing with methanol/water was significantly higher than that prepared by rinsing with DI water. This higher deposition was likely due to the formation of β-sheet structure in silk layers mediated by the dehydration impact of methanol which stabilized the films, limiting the desorption of the model compound Rhodamine B from the film. This structural transition induced by methanol is commonly used to stabilize silk fibroin in various forms including films.[18] We previously reported that the silk II (β-sheet) structure could be formed via the dehydration effects with nitrogen gas, even without methanol treatment, although a lower crystalline content was attained. In the present study, rinsing the deposited films in pure water resulted in partial desorption of silk fibroin and the Rhodamine B molecules, resulting in the lower deposition values. The control of β-sheet structure could be used to regulate the diffusion rate of the incorporated compounds in the silk film to achieve controlled release.

The real-time adsorption of model compounds on silk pre-coated gold electrode surfaces was monitored using research quartz crystal microbalance (RQCM). Representative *in situ* mass changes as a function of time for the adsorption of Rhodamine B, Even Blue, and Azoalbumin on the silk pre-coated RQCM gold electrode surface are shown in Figure 4. All the samples typically exhibit a very rapid initial deposition phase, followed by a slower phase upon approaching a steady state. However, small molecule compounds reached the steady state faster than the larger protein; almost 92% and 82% of the adsorption (saturation) took place within the first 2 min for small molecules (Rhodamine and Even Blue) and protein, respectively. Rhodamine B had a higher adsorption on silk coating than Even Blue.

In our previous study, we exploited the strong hydrophobic interactions characteristic of silk fibroin as the basis for film stabilization. Silkworm silk fibroin from *B. mori* consists about 60% of glycine and alanine repeats that dominate the structure.[30] The fibroin chain consists

primarily of two polypeptide block sequences, crystalline (hydrophobic) and less ordered blocks (hydrophilic and smaller in size) that alternate regularly. The basic sequence of the crystalline block is of -(Ala-Gly)$_n$- that adopts a β-sheet structure, whereas the less ordered blocks contain additional amino acids, in particular tyrosine and valine.[31] In a silk fibroin dilute solution system, the driving forces for the deposition of the silk fibroin protein chains onto a solid substrate are attributed to hydrophobic interactions as well as partial electrostatic interactions.[12] The incorporation of the dye model compounds into the silk fibroin layers could also be driven by hydrophobic interactions as well as electrostatic interactions. At neutral pH, the silk fibroin has a net negative charge due to an isoelectric point of 4.03 in the hydrophilic domains and of 4.59 in the N-terminal domains.[32] However, patches of positively charged domains are also existent in the C-terminal domains. The model compounds used in this study were charged amphiphilic molecules which have charged groups as well as hydrophobic aromatic groups which can be assumed to participate in the overall assembly process. The assumption was supported by the observation that the adsorption could be achieved in a wide range of pH (2.0 to 11) regardless the net charge sign of the compound and silk fibroin. However, when the net charge on silk and the compound solutions are opposite, greater adsorption was observed. This can be explained by considering that the interactions related to the incorporation of model compounds into the silk fibroin layer are likely to reflect a balance between different factors such as hydrophobic and electrostatic interactions, depending on the structure of the molecules and the environmental conditions employed during the deposition process. In this study, all of the deposition procedures were carried out at pH 7.0 ~ 7.5. The ability to construct the multilayered thin films at neutral pH would be useful for some biomedical devices and also in a therapeutic context related to the incorporation of labile drugs.

3.2. Structure and morphology of the films

The understanding and control of the silk fibroin coating structure and morphology to regulate the release behavior of the incorporated components is important. Silk proteins are characterized by nanodomains, based on the highly repetitive primary sequence and hydrophobic nature of these sequences, and the subsequent protein assembly during processing that leads to the formation of characteristic β-sheet secondary structures.[31] Several models have been proposed for the secondary structure of silk fibroin, including random coil, α-helix, silk I, silk II, and silk III. Random coil and *α*-helix tend to be lumped into silk I since they cannot be distinguished by infrared spectroscopy.[33] Silk II is an antiparallel β-sheet in which the polypeptide chains are aligned and adjacent chains are connected with hydrogen bonds between carbonyl and amine groups. Silk I is a less condensed structure than silk II but is usually considered highly metastable and will convert to silk II (*β*-sheet) by physicochemical treatments such as the application of mechanical forces (stretching, shearing, rolling, spinning, or compressing), thermal treatment,[34] and immersion in selected organic solvents such as methanol.[35] In native *B. mori* silkworm silk fibers, approximately 62–65% beta sheet content is reported. In our prior nanolayer deposition work, we reported up to 40% *β*-sheet content induced during the nitrogen drying process from FTIR spectroscopy,[12] likely due to dehydration effects, as is also observed with methanol treatment.

In the present study, the structures of the films with various multilayer structures and treatment methods were investigated by X-ray diffraction analysis. Figure 5a and 5b show the wide angle X-ray diffraction profiles of the Rhodamine B and Azoalbumin loaded silk films with two different multilayer structures, each with and without methanol treatment (1-A, B, C, D and 3-A, B, C, D); along with amorphous silk cast film for comparison as a control. Clearly defined peaks at about 21° and a shoulder at about 24° corresponding to the β–sheet crystalline form are shown for all the samples. These results indicate d-crystalline spacings of 0.435 and 0.37 nm according to the 21° and 24° reflections, respectively using $\lambda = 0.154$ nm.[36] Assuming the diffraction pattern of silk film cast from aqueous solution as non-crystalline, the calculated

crystallinity index of each sample is shown in Table 2. As expected, the silk II (*β*-sheet) structure formed even without methanol treatment as was reported in our previous study.[12] The formation of the silk II structure under aqueous condition was attributed to the nitrogen gas drying process which may have dehydrated the structure, inducing the β-sheet formation (silk II). Further increased crystalline index after methanol treatment in each sample indicated the stronger effect of methanol treatment on β-sheet formation. The incorporation of small molecules as well as proteins did not perturb the crystal structure in silk, suggesting the coexistence of silk and compound domains in the films. It is worth noting that X-ray diffractometry is more qualitative in a significantly amorphous systems like in the present study. The crystalline content shows a relatively large discrepancy when compared with previous studies, due to the difference in X-ray diffractometry vs. FTIR spectroscopy. FTIR spectroscopy is sensitive to short-range order while X-ray diffractometry is sensitive to long-range order.[37] Since X-ray diffractometry mainly detects the interplanar spacings of crystallites, the crystallinity index calculated from X-ray diffractogram is lower when compared with other techniques.[34,38]

The surfaces of the films were characterized by AFM. Tapping mode AFM micrographs of 1 μm^2 sections of two samples: $(silk/RH)_6$-silk and $(silk/AA)_6$-silk before and after immersion of the samples in PBS for 24 h are shown in Figure 6. There were no obvious differences in surface morphology when comparing samples with and without methanol treatment, in which a similar globular structure was adopted. However, this globular surface morphology was only observed in methanol treated cast silk film but was absent in water vapor treated cast silk film in a previous publication,[20] indicating a more heterogeneous morphology in multilayer silk films. The topographic surface roughness (RMS) for $(silk/RH)_6$-silk film before and after immersion of the samples in PBS for 24 h samples at a measured size of 1.0×1.0 μm^2 were similar, with average values of 5.45 nm and 5.69 nm, respectively. However, the phase roughness increased significantly after the immersion of the samples, from 3.38° to 8.94°. For $(silk/AA)_6$-silk, both the topographic surface roughness (RMS) and the phase roughness increased considerably, from 2.99 nm to 4.47 nm and 4.89° to 12.12°, respectively. No significant changes in roughness were observed for the silk-only surface. The increased roughness in phase images for model compound-loaded silk surfaces could be explained in that the diffusion of the model compounds to the topmost layer caused the silk protein molecules to undergo structural rearrangements; small molecule compounds had less effect on the surface topographic features than the protein model compound. However, this speculation needs to be further confirmed by evaluating the crystalline nature of the silk films after the release of the model compounds.

The thickness of the films was measured with the AFM analysis at the film edge area. Figure 7 shows the measurement of the film thickness of $(silk/Rh)_6$-silk. Two distinct heights are observed and the thickness was obtained from the value of the step height, 33.0 nm. The thicknesses of $(silk/AA)_6$-silk was 68.4 nm using the same measurement method. The higher overall thickness of azo-albumin systems than rhodmine-B systems could be due to the loops and tails formed upon deposition of the macromolecular chains of albumin. These loops and tails would result in thicker layers than those of small molecules with the same number of layers.

3.3. In vitro release studies

The effect of the multilayer structure and the crystalline structure of the film on model compound release profiles was investigated. The released behaviors of Rhodamine B from multilayer silk films in PBS solution with different multilayer structures and treatment methods are shown in Figure 8A. All the curves followed a similar release profile, an initial burst followed by a slower and steadier release. However, the initial burst was significantly

suppressed and the duration of the completion of the release was considerably prolonged by treating the films with methanol and adding 6 barrier layers of silk fibroin. For example, the films $(silk/RH)_6$-silk prepared by rinsing with water and methanol had a initial burst of 72.5% and 57.1% in the first 6 h, and a 100% release after 14 days and 16 days respectively. These data indicate that the higher crystalline content induced by methanol treatment decreased the release rate. The films $(silk/RH)_6$-$silk_6$ prepared by rinsing with water and methanol had a initial burst of 44.2% and 32.0% in the first 6 h and a 100% release at 30 and 35 days, respectively. The further decrease in the release rate was attributed to higher crystallinity and barrier hindrance by adding more silk layers.

Similar release behavior was observed for azoalbumin loaded coatings with various multilayer structure and treatment methods (Figure 8B). For all the samples, the initial burst in the first 6 h was much lower (<6.5%) than for the small molecule-immobilized samples. The time to release 100% of the incorporated azoalbumin increased from 21 to 35 days by adding 3 barrier layers of silk fibroin and using the methanol treatment. These results agree with our previous study with cast silk films, which demonstrated that crystalline β-sheets induced by methanol treatment resulted in a concomitant decrease in water solubility and more sustained release kinetics for model protein incorporated silk films.

The semi-empirical power law equation introduced by Siepmann and Peppas[39] was used to quantify release behavior, as given below:

$$M_t/M_\infty = kt^n,$$

where M_t/M_∞ is the fractional amount of the drug released at time t, k is a characteristic constant of the system, and exponent n describes the kinetics and the release mechanism, which depends on the geometry of the system. In the case of pure Fickian release, the exponent n has the limiting values of 0.50 in a slab system. On the other hand, when n = 1, a zero-order release or Case II transport is suggested. Other values for n indicate anomalous transport kinetics,[40] a combined mechanism of pure diffusion and Case II transport. In order to obtain a linear fit for the drug release data, the above equation can be modified as shown below:

$$\log(\text{released}\%) = \log(M_t/M_\infty) = \log k + n \log t,$$

where n can be obtained from the slope of the plot of log(released%) versus log t by linear fitting. Due to the approximate character the use of the equation has been confined to the description of the first 60% of the release curve.[41] Recently, Rinaki *et al.* validated the hypothesis that the power law can describe the entire release profile of several drug release studies from hydroxypropyl methylcellulose-based delivery systems.[42] In this study, attempt to use the modified equation above was made to analyze the release profiles excluding the initial burst region as shown in Figure 9A and 9B. It is interesting that the experimental data had a fairly good linear fit for both Rhodmine B and Azoalbumin release from post-initial burst stage up to 100% release. The values of diffusional exponent (n), correlation coefficient (r^2), and release rate coefficients (k) obtained are summarized in Table 3. It is shown that the exponent n values for the release of rhodamine B were within the limiting value of 0.5 (0.078, 0.134, 0.27, and 0.377 for sample 1A to 1D), suggesting a Fickian release behavior. In the case of azoalbumin, exponent values of slightly higher than 0.5 (0.509, 0.5724, 0.506, and 0.551 for 3A to 3D) were observed. This result resembled a complex combination of pure diffusion and Case II transport in which Fickian release behavior dominated. More work is needed to fully understand the mechanism of release. The data provide interesting information about the multilayered silk thin film systems and represents a platform from which the controlled release

of other coating structures and drug types (i.e., therapeutically used proteins or small molecule drugs) can be explored.

4. Summary

The feasibility of construction and drug release of LbL silk fibroin coatings was assessed, with both small molecule drugs and therapeutically relevant proteins. The amount of immobilized compounds could be controlled by changing the dipping solution concentration, pH and the rinsing method, with linear control. Suppression of the initial burst and prolonging the duration of release of these incorporated molecules was achieved by controlling the coating structure, such as inducing crystalline structure and adding silk barrier layers to hinder release. In light of previous investigations of the pharmaceutical utility of silk fibroin materials for drug delivery, the novel coating materials and surface modification approaches reported here offer an attractive framework for controlled release from surface engineered biomaterials and medical devices. While a single drug was the focus in the present work, the technology can easily be extended to multi-drug release profiles with the required control via multi-step depositions.

Acknowledgments

This work was supported by NIH (EB002520 and EB003210) and the NSF (DMR). We thank Anthony B. Barry, Wyeth BioPharma, for his critical assessment of this work. We also thank Ms. Yenhsi Lin, surface engineering and molecular assembly laboratory, Iowa State University, for assistance with the coating thickness measurements.

References

1. Fredin NJ, Zhang J, Lynn DM. Surface analysis of erodible multilayered polyelectrolyte films: nanometer-scale structure and erosion profiles. Langmuir 2005;21(13):5803–5811. [PubMed: 15952826]
2. Forzani ES, Perez MA, Lopez Teijelo M, Calvo EJ. Redox driven swelling of layer-by-layer enzyme-polyelectrolyte multilayers. Langmuir 2002;18(25):9867–9873.
3. Thierry B, Winnik FM, Merhi Y, Silver J, Tabrizian M. Bioactive coatings of endovascular stents based on polyelectrolyte multilayers. Biomacromolecules 2003;4:1564–1571. [PubMed: 14606881]
4. Zhu H, McShane MJ. Loading of hydrophobic materials into polymer particles: implications for fluorescent nanosensors and drug delivery. J Am Chem Soc 2005;127(39):13448–13449. [PubMed: 16190679]
5. Hammond P. Form and function in multilayer assembly: new applications at the nanoscale. Adv Mater 2004;16:1271–1293.
6. Decher G, Hong JD, Schmitt J. Buildup of ultrathin multilayer films by a self-assembly process: III. Consecutively alternating adsorption of anionic and cationic polyelectrolytes on charged surfaces. Thin Solid Films 1992;210/211:831–835.
7. Decher G. Fuzzy Nanoassemblies: toward layered polymeric multicomposites. Science 1997;29(277): 1232–1237.
8. Chung AJ, Rubner MF. Methods of loading and releasing low molecular weight cationic molecules in weak polyelectrolyte multilayer films. Langmuir 2002;18:1176–1183.
9. Sukhishvili SA, Granick S. Layered, Erasable polymer multilayers formed by hydrogen-bonded sequential self-assembly. Macromolecules 2002;35(1):301–310.
10. Wood KC, Boedicker JQ, Lynn DM, Hammond PT. Tunable drug release from hydrolytically degradable layer-by-layer thin films. Langmuir 2002;21:1603–1609. [PubMed: 15697314]
11. Recksiedler CL, Deore BA, Freund MS. A novel layer-by-layer approach for the fabrication of conducting polymer/RNA multilayer films for controlled release. Langmuir 2006;22:2811–2815. [PubMed: 16519487]
12. Wang X, Kim HJ, Xu P, Matsumoto A, Kaplan DL. Biomaterial coatings by stepwise deposition of silk fibroin. Langmuir 2005;21(24):11335–11341. [PubMed: 16285808]

13. Altman GH, Diaz F, Jakuba C, Calabro T, Horan RL, Chen J, Lu H, Richmond J, Kaplan DL. Silk-based biomaterials. Biomaterials 2003;24:401–416. [PubMed: 12423595]
14. Panilaitis B, Altman GH, Chen J, Jin HJ, Karageorgiou V, Kaplan DL. Macrophage responses to silk. Biomaterials 2003;24(18):3079–3085. [PubMed: 12895580]
15. Meinel L, Karageorgiou V, Hofmann S, Fajardo R, Snyder B, Li C, Zichner L, Langer R, Vunjak-Novakovic G, Kaplan DL. Engineering bone-like tissue in vitro using human bone marrow stem cells and silk scaffolds. J Biomed Mater Res A 2004;71(1):25–34. [PubMed: 15316936]
16. Nazarov R, Jin HJ, Kaplan DL. Porous 3D scaffolds from regenerated silk fibroin. Biomacromolecules 2004;5:718–726. [PubMed: 15132652]
17. Kim UJ, Park J, Li C, Jin HJ, Valluzzi R, Kaplan DL. Structure and properties of silk hydrogels. Biomacromolecules 2004;5:786–92. [PubMed: 15132662]
18. Jin HJ, Park J, Karageorgiou V, Kim UJ, Valluzzi R, Cebe P, Kaplan DL. Water-stable silk films with reduced β-sheet content. Adv Funct Mater 2005;15(8):1241–1247.
19. Horan RL, Antle K, Collette AL, Wang Y, Huang J, Moreau JE, Volloch V, Kaplan DL, Altman GH. In vitro degradation of silk fibroin. Biomaterials 2005;26:3385–3393. [PubMed: 15621227]
20. Hofmann S, Foo CW, Rossetti C, Textor M, Merkle HP, Kaplan DL, Meinel L. Silk fibroin as an organic polymer for controlled drug delivery. J Controlled Release 2006;111:219–227.
21. Bayraktar O, Malay O, Ozgarip Y, Batgun A. Silk fibroinas a novel coating material for controlled release of theophylline. Eur J Pharm Biopharm 2005;60:373–381. [PubMed: 15996578]
22. Katayama H, Issiki M, Yoshitomi H. Application of fibroin in controlled release tablets containing theophylline. Biol Pharm Bull 2000;23(10):1229–1234. [PubMed: 11041257]
23. Rujiravanit R, Kruaykitanon S, Jamieson AM, Tokura S. Preparation of cross-linked chitosan/silk fibroin blend films for drug delivery system. Macromol Biosci 2003;3(10):604–611.
24. Kim UJ, Park JH, Kim HJ, Wada M, Kaplan DL. Three-dimensional aqueous-derived biomaterial scaffolds from silk fibroin. Biomaterials 2005;26:2775–2785. [PubMed: 15585282]
25. Kumaraswamy G, Verma RK, Kornfield JA, Yeh F, Hsiao BS. Shear-enhanced crystallization in isotactic polypropylene. in-situ synchrotron SAXS and WAXD. Macromolecules 2004;37:9005–9017.
26. Xu H, Cebe P. Transitions from solid to liquid in isotactic polystyrene studied by thermal analysis and X - ray scattering. Polymer 2005;46(20):8734–8744.
27. Wang ZG, Hsiao BS, Sirota EB, Agarwal P, Srinivas S. Probing the early stages of melt crystallization in polypropylene by simultaneous small- and wide-angle x-ray scattering and laser light scattering. Macromolecules 2000;33:978–989.
28. Lvov Y, Ariga K, Ichinose I, Kunitake T. Assembly of multicomponent protein films by means of electrostatic layer-by-layer adsorption. J Am Chem Soc 1995;117:6117–6122.
29. He JA, Samuelson L, Li L, Kumar J, Tripathy SK. Oriented bacteriorhodopsin/polycation multilayers by electrostatic layer-by-layer assembly. Langmuir 1998;14(7):1674–1679.
30. Fraser, RDB.; MacRae, TP., editors. Conformation in fibrous proteins and related synthetic polypeptides. Academic Press; New York: 1973. p. 94-125.Chapter 5
31. Bini E, Knight DP, Kaplan DL. Mapping Domain Structures in Silks from Insects and Spiders Related to Protein Assembly. J Mol Biol 2004;335:27–40. [PubMed: 14659737]
32. Wong Po FC, Bini E, Hensman J, Knight DP, Lewis RV, Kaplan DL. Role of pH and charge on silk protein assembly in insects and spiders. Applied Physics - Section A - Materials Science and Processing 2006;82(2):223–234.
33. Asakura T, Kuzuhara A, Tabeta R, Saito H. Conformational characterization of Bombyx mori silk fibroin in the solid state by high-frequency carbon-13 cross polarization-magic angle spinning NMR, x-ray diffraction, and infrared spectroscopy. Macromolecules 1985;18:1841–1845.
34. Hu X, Kaplan D, Cebe P. determining beta-sheet crystallinity in fibrous proteins by thermal analysis and infrared spectroscopy. Macromolecules 2006;39:6161–6170.
35. Nam J, Park YHJ. Morphology of regenerated silk fibroin: Effects of freezing temperature, alcohol addition, and molecular weight. Appl Polym Sci 2001;81:3008–3021.

36. Magoshi J, Mizuide M, Magoshi Y, Takahashi K, Kubo M, Nakamura S. Physical properties and structure of silk. VI. Conformational changes in silk fibroin induced by immersion in water at 2 to 130°C. J Polym Sci B: Polym Phys 1979;17(3):515–520.

37. Koenig, JL.; Kendall, DN., editors. Applied infrared spectroscopy. New York: Reinhold; 1966. p. 245

38. Um IC, Kweon HY, Park YH, Hudson S. Structural characteristics and properties of the regenerated silk fibroin prepared from formic acid. Intern J Biological Macromolecules 2001;29:91–97.

39. Siepmann J, Peppas NA. Modeling of drug release from delivery systems based on hydroxypropyl methylcellulose (HPMC). Adv Drug Delivery Rev 2001;48:139–157.

40. Ritger PL, Peppas NA. A simple equation for description of solute release. I. fickian and non-fickian release from non-swellable devices in the form of slabs, spheres, cylinders or discs. J Controlled Release 1987;5:23–36.

41. Korsmeyer RW, Gurny R, Doelker E, Buri PA, Peppas NA. Mechanisms of solute release from porous hydrophilic polymers. Intern J Pharm 1983;15:25–35.

42. Rinaki E, Valsami G, Macheras P. The power law can describe the ‘entire’ drug release curve from HPMC-based matrix tablets: a hypothesis. Intern J Pharm 2003;255:199–207.

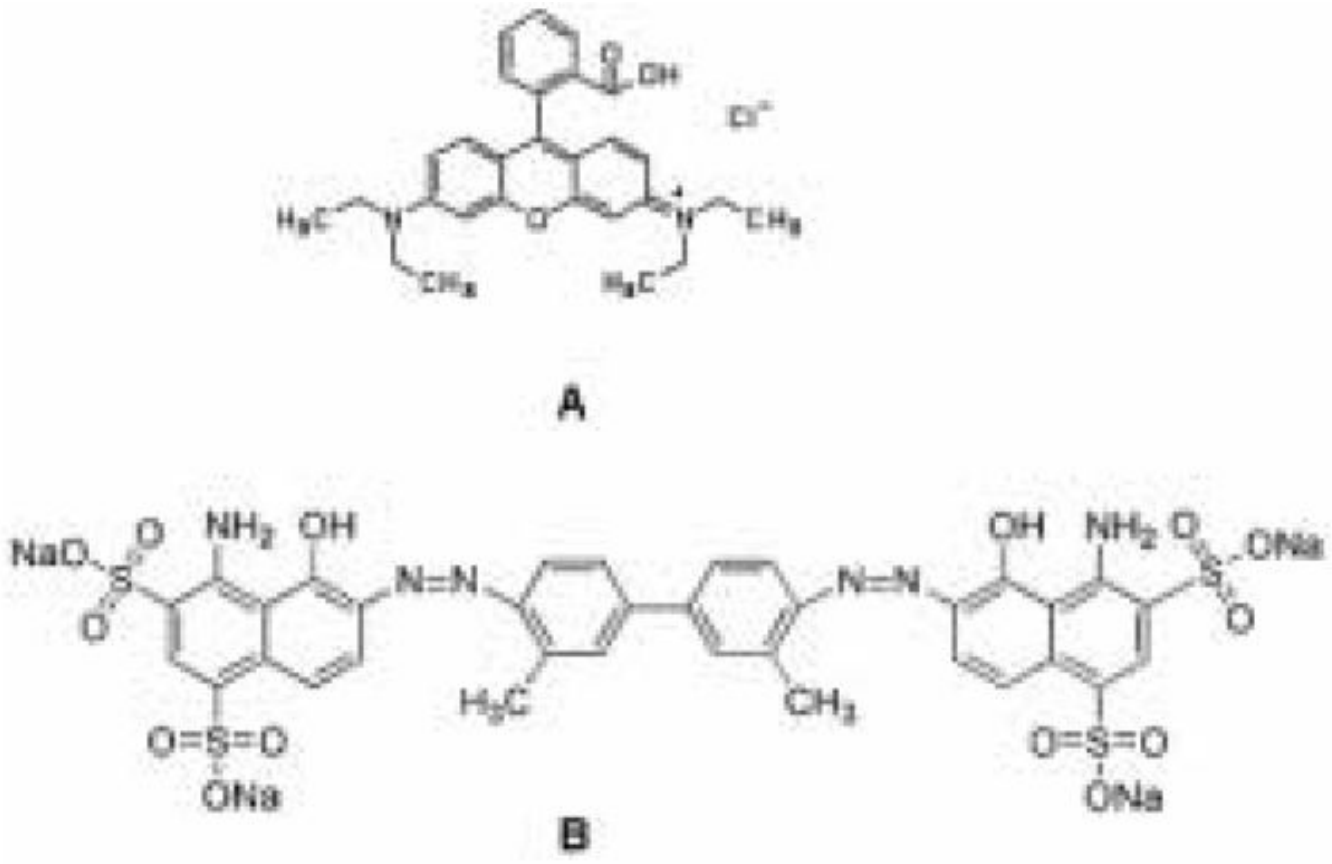

Figure 1.
Structures of small molecule drug model compounds: (A) Rhodamine B; (B) Even Blue.

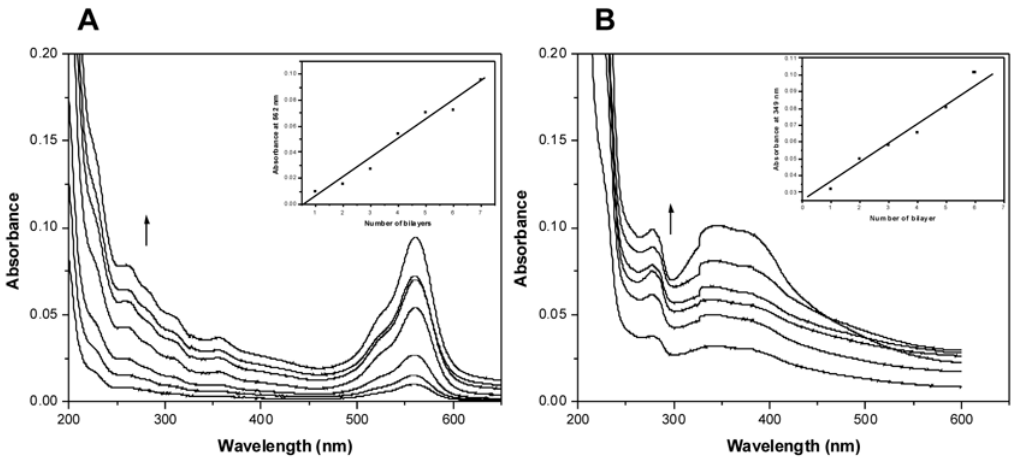

Figure 2.

UV-Vis absorption spectra of (A) $(silk/RH)_n$ and (B) $(silk/AA)_n$ multilayered thin films on quartz slides as a function of the number of bilayers. The arrows indicate the increase of the number of bilayers. The insets show linear increases of the characteristic absorption peaks of Rhodamine B and Azoalbumin in A and B, respectively. Note: RH=Rhodamine B; AA=Azoalubmin.

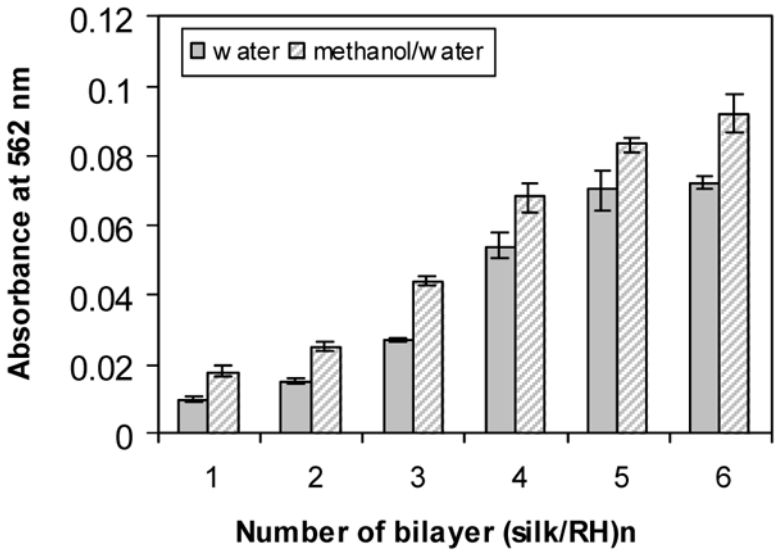

Figure 3.

UV-Vis absorbance at 562 nm of $(silk/RH)_n$ on quartz slides as a function of the bilayer number and rinse stabilization method. Absorbance values were recorded at 3 different locations on the substrate.

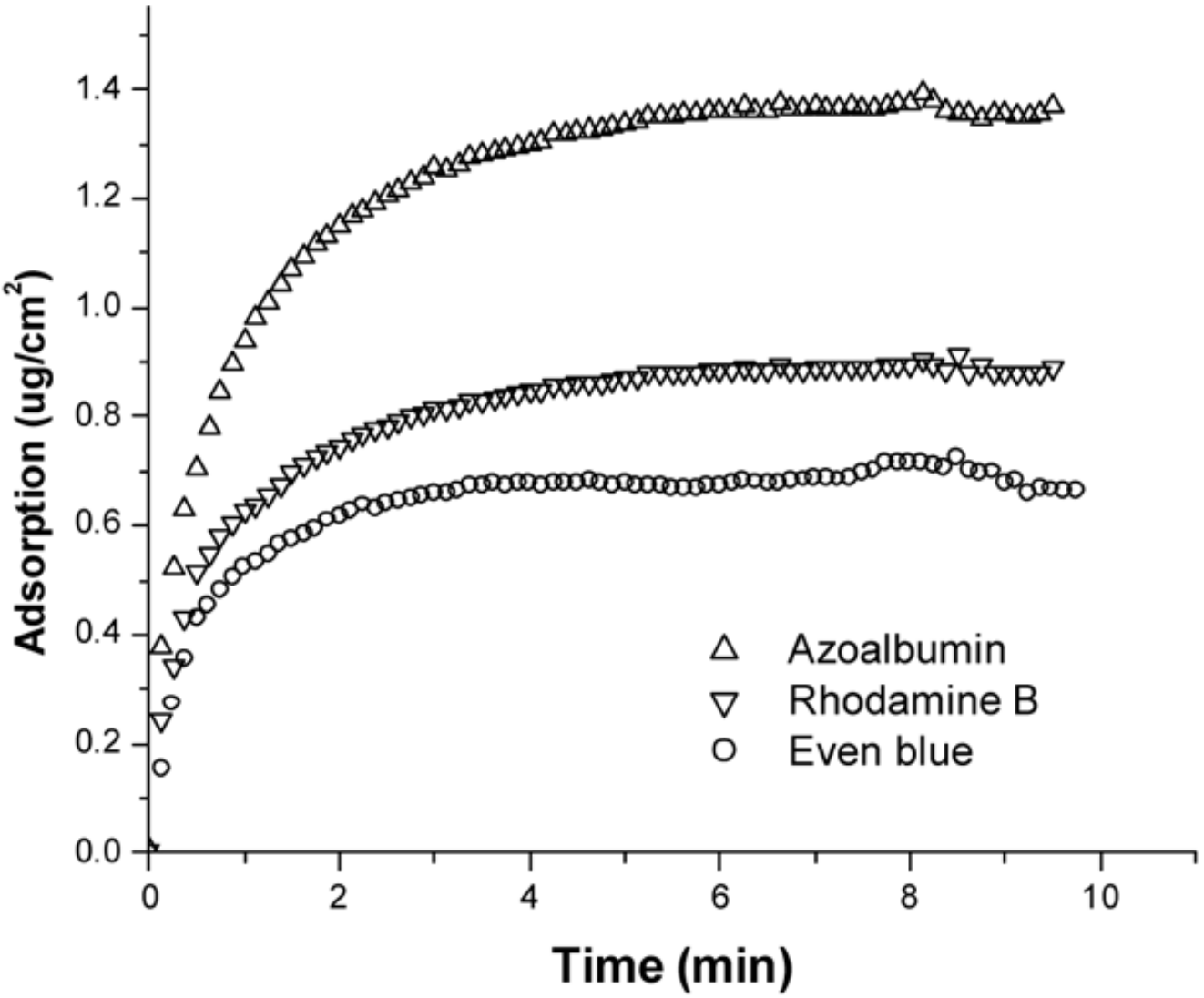

Figure 4.
Real-time monitoring of the deposition of model compounds on silk pre-coated gold electrode using a research quartz crystal microbalance (RQCM).

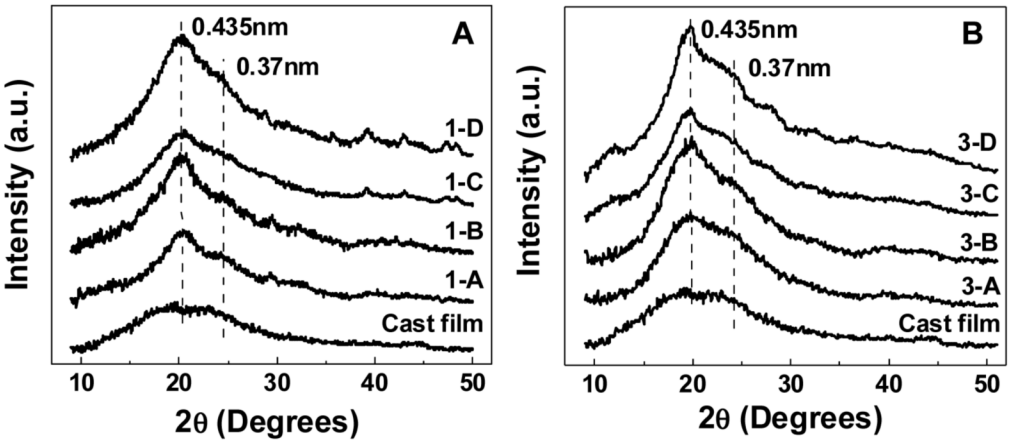

Figure 5.
X-ray diffraction profiles (λ = 0.154 nm) of multilayer thin films with various compositions and treatment methods: (A) Rhodamine B incorporated silk films; (B) Azoalbumin-incorporated silk films. The description of the samples is shown in Table 1. The cast film was used as a non-crystalline control.

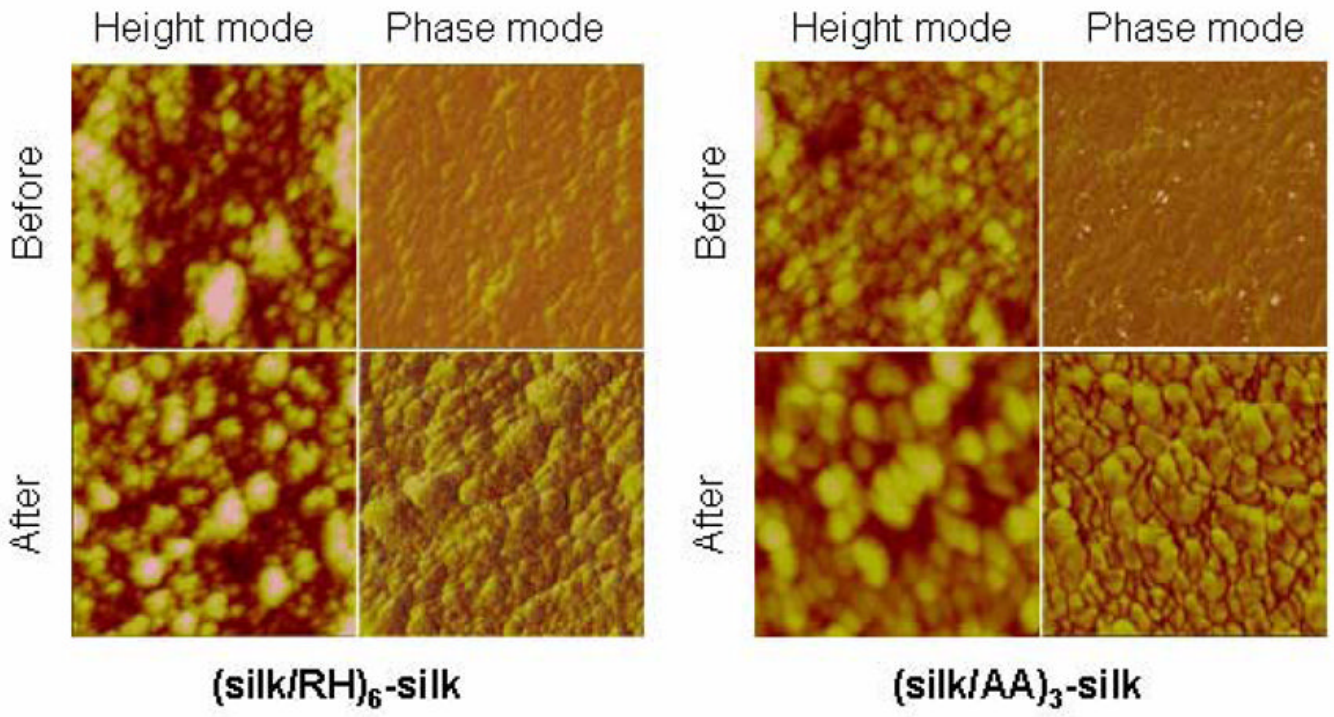

Figure 6.
AFM height mode and phase mode images in air obtained for (silk/RH)$_6$-silk and (silk/AA)$_6$-silk on mica wafer before and after immersion of the samples in PBS for 24 h. Each image is 1 μm × 1 μm. RH=Rhodamine B; AA=Azoalbumin.

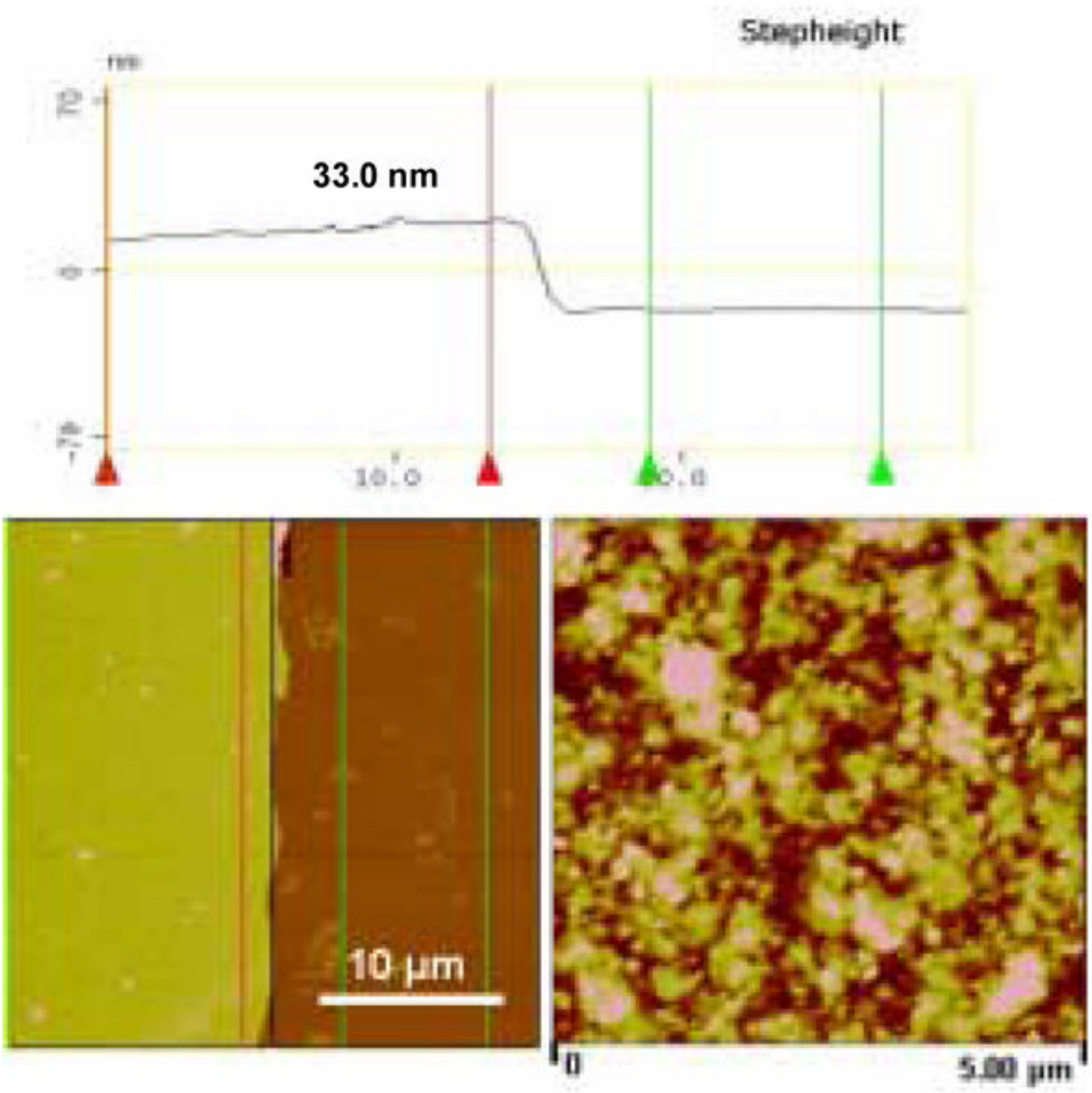

Figure 7.
AFM cross-section analysis at the film edge area to obtain film thickness of $(silk/Rh)_6$-silk.

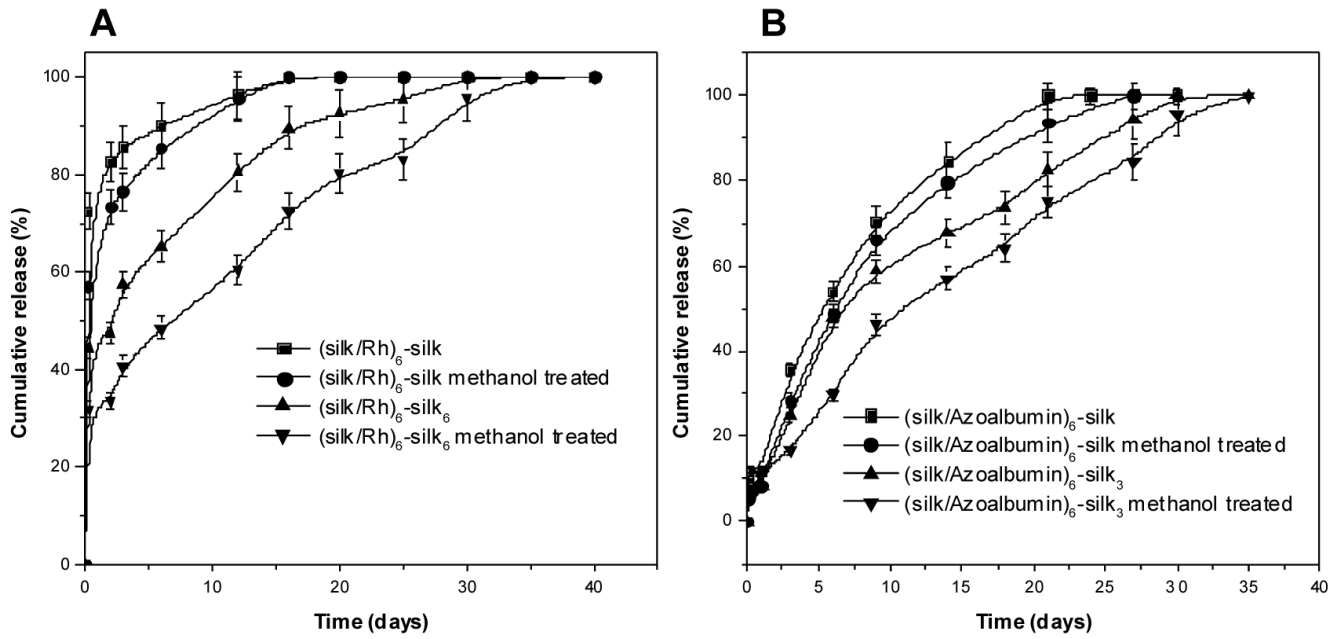

Figure 8.
Cumulative release profiles of Rhodamine B-incorporated silk films (A) and Azoalbumin-incorporated silk films (B) with various multilayer structures and treatment methods.

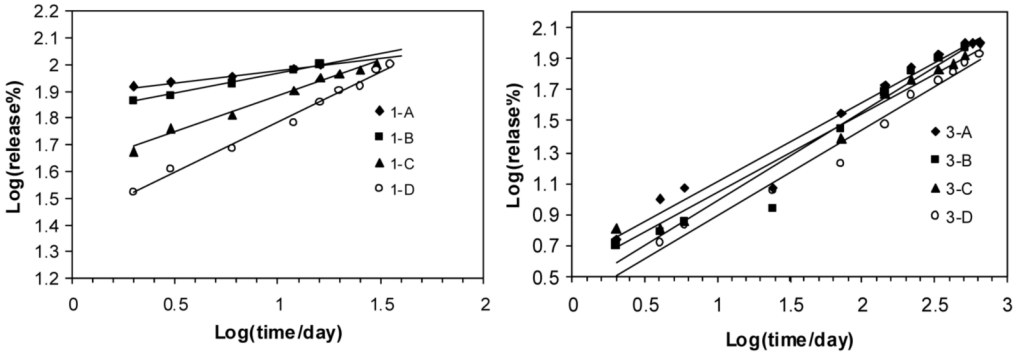

Figure 9.
The experimental data based on the power law model for Rhodamine B (left) and Azoalbumin (right) released from different silk multilayered structures. A linear relationship was observed for each sample.

Table 1

Multilayer film samples in the release study

Model compound	Sample	Multilayer structure	Film treatment
Rhodamine B (RH)	1-A	$(silk/RH)_6$-silk	--
	1-B	$(silk/RH)_6$-silk	Methanol
	1-C	$(silk/RH)_6$-$silk_6$	--
	1-D	$(silk/RH)_6$-$silk_6$	Methanol
Even Blue (EB)	2-A	$(silk/EB)_6$-silk	--
	2-B	$(silk/EB)_6$-silk	Methanol
	2-C	$silk/EB)_6$-$silk_6$	--
	2-D	$(silk/EB)_6$-$silk_6$	Methanol
Azoalbumin (AA)	3-A	$(silk/AA)_6$-silk	--
	3-B	$(silk/AA)_6$-silk	Methanol
	3-C	$(silk/AA)_6$-$silk_3$	--
	3-D	$(silk/AA)_6$-$silk_3$	Methanol

Note: RH = Rhodamine B; EB = Even Blue; AA = Azoalbumin. The subscript corresponds to the number of layers therein.

Table 2

Crystalline index(%) from WAXD analysis

Model compound	Sample	Composition	Film treatment	Crystalline index (%)
Rhodamine B (RH)	1-A	$(silk/RH)_6$-silk	--	19.2~22.2
	1-B	$(silk/RH)_6$-silk	Methanol	22.3~26.1
	1-C	$(silk/RH)_6$-$silk_6$	--	18.8~21.8
	1-D	$(silk/RH)_6$-$silk_6$	Methanol	27.6~30.2
Azoalbumin (AA)	3-A	$(silk/AA)_6$-silk	--	6.88~8.76
	3-B	$(silk/AA)_6$-silk	Methanol	19.3~22.9
	3-C	$(silk/AA)_6$-$silk_3$	--	12.6~18.0
	3-D	$(silk/AA)_6$-$silk_3$	Methanol	26.2~28.4

Table 3

Drug release parameters obtained from the modified Peppas equation

Model compound	Sample	n	r^2	k
Rhodamine B (RH)	1-A	0.078	0.986	1.901
	1-B	0.134	0.993	1.831
	1-C	0.27	0.988	1.611
	1-D	0.377	0.989	1.407
Azoalbumin (AA)	3-A	0.509	0.957	0.062
	3-B	0.5724	0.967	0.415
	3-C	0.506	0.982	0.542
	3-D	0.551	0.979	0.343